

Antiferromagnetic and structural transitions in the superoxide KO_2 from first principles: A $2p$ -electron system with spin-orbital-lattice coupling

Minjae Kim, Beom Hyun Kim, Hong Chul Choi, and B. I. Min

Department of Physics, PCTP, Pohang University of Science and Technology, Pohang, 790-784, Korea

(Dated: November 6, 2018)

KO_2 exhibits concomitant antiferromagnetic (AFM) and structural transitions, both of which originate from the open-shell $2p$ electrons of O_2^- molecules. The structural transition is accompanied by the coherent tilting of O_2^- molecular axes. The interplay among the spin-orbital-lattice degrees of freedom in KO_2 is investigated by employing the first-principles electronic structure theory and the kinetic-exchange interaction scheme. We have shown that the insulating nature of the high symmetry phase of KO_2 at high temperature (T) arises from the combined effect of the spin-orbit coupling and the strong Coulomb correlation of O $2p$ electrons. In contrast, for the low symmetry phase of KO_2 at low T with the tilted O_2^- molecular axes, the band gap and the orbital ordering are driven by the combined effects of the crystal-field and the strong Coulomb correlation. We have verified that the emergence of the O $2p$ ferro-orbital ordering is essential to achieve the observed AFM structure for KO_2 .

PACS numbers: 75.50.Ee, 71.70.Ej, 71.15.Mb

Magnetism due to the correlated $2p$ electrons has attracted revived attention for the possibility of the new kinds of the magnetic informative materials.^{1,2} Some $2p$ magnetic oxides exhibit the structural phase transition concomitantly with the magnetic phase transition.^{3,4,5} Solid oxygen is a typical example, which has both antiferromagnetic (AFM) and structural phase transitions below 24 K.³ Alkali superoxides, AO_2 ($A=\text{Na}, \text{K}, \text{Rb}$), which are of our present interest, belong to another example.^{2,6} In AO_2 , one alkali-metal atom provides one electron to an oxygen molecule, and thereby each O_2^- anion has nine electrons at the $2p$ molecular levels with the electronic configuration of $\sigma_g^2\pi_u^4\pi_g^3$ (see the inset of Fig. 2).^{1,7} The partially occupied antibonding π_g molecular states play the most important role in determining the electronic and magnetic properties of alkali superoxides.⁸ One hole in π_g generates the magnetic moment of $1 \mu_B$ for each O_2^- . The degeneracy of the π_g level is expected to be lifted by lowering the crystal symmetry, as occurs due to the Jahn-Teller effect.⁸ In fact, it was suggested that, for KO_2 , the symmetry lowering would occur *via* coherent tilting of the O_2^- molecular axes, the so-called magnetogyration, which invokes the accompanying AFM ordering.^{4,5,9}

At room temperature, KO_2 crystallizes in the tetragonal structure of CaC_2 type, in which the O_2^- molecular bond axes are parallel to the z -axis (Fig. 1(a)).⁴ KO_2 retains this structure down to 197 K and exhibits the paramagnetic behavior. Upon cooling, O_2^- molecular bond axes seem to tilt uniformly by $\sim 20^\circ$ to have a lower crystal (monoclinic) symmetry. The magnetic phase is still paramagnetic down to 7 K. Below 7 K, the AFM ordering emerges in the triclinic crystal structure with the uniform tilting of O_2^- molecular bond axes by $\sim 30^\circ$.⁴ According to neutron experiment,¹⁰ the AFM phase has the magnetic structure having opposite spin arrangements along the z -direction between two oxygen layers of O1 and O2. This feature in KO_2 reflects the

strong interplay among spin, orbital, and lattice degrees of freedom, as in rare-earth manganites.²

There have been several theoretical reports to study the coupled structural and magnetic transitions in KO_2 ,^{2,8,9,11,12} but those studies were mostly qualitative and lacked the quantitative description of the electronic structures for the low symmetry phase of KO_2 . Even the direction of the tilted molecular bond axis is still uncertain between two possibilities. The first one is [R1] in Fig. 1(b), in which the molecular bonds are rotated around the [100] axis. The second one is [R2] in Fig. 1(c), in which the molecular bonds are rotated around [110] axis. Moreover, the recent band structure study for the high symmetry phase of KO_2 (Fig. 1(a)) in the local density approximation (LDA)² reveals that the degenerate π_g states do not split, resulting in the metallic nature, which is contradictory to the insulating nature of KO_2 .

In this Rapid Communication, we have investigated comprehensively the electronic structures of both high and low symmetry phases of KO_2 , and explored the

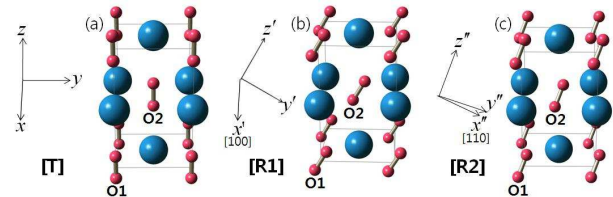


FIG. 1: (Color online) (a) The tetragonal [T] structure of KO_2 with unrotated O_2^- molecular bond axes. The molecular axes are along the z -direction. K atoms are in blue and O atoms in red. (b) [R1] with molecular bonds rotated by $\sim 30^\circ$ around the [100] (x') axis with bond axes along the z' -direction. (c) [R2] with molecular bonds rotated by $\sim 30^\circ$ around the [110] (x'') axis with bond axes along the z'' -direction. There are two independent types of oxygen O1 and O2 for each structure.

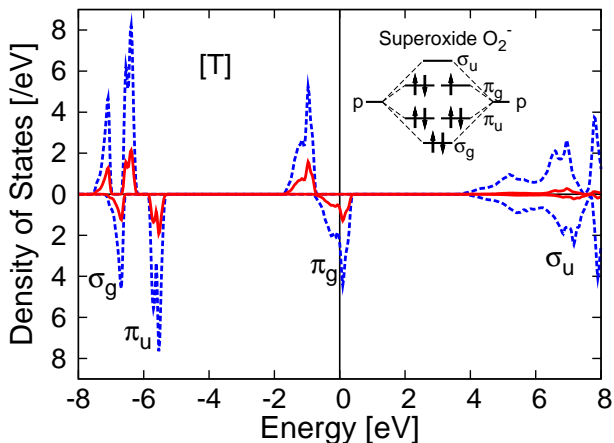


FIG. 2: (Color online) The DOS in the GGA for the FM phase of KO_2 with [T] structure. Dotted (blue) and solid (red) lines represent the total DOS and the partial DOS of oxygen $2p$ states, respectively. The upper and the lower panels correspond to the majority and minority spin DOSs. Inset shows the $2p$ molecular levels of O_2^- .

mechanism of the interplay between the spin and lattice degrees of freedom in correlated $2p$ electron systems. Further, we have examined the origins of the band gap opening and the exchange interactions between O_2^- molecules in KO_2 .

We have employed the full-potential augmented plane wave (FLAPW) band method¹³ implemented in WIEN2k package.¹⁴ For the exchange-correlation potential, the generalized gradient approximation (GGA)¹⁵ was used. We also incorporate the on-site Coulomb interaction U between the oxygen $2p$ electrons (GGA+ U) and the spin-orbit (SO) effect as a second variational procedure (GGA+ U +SO). The valence wave functions inside the muffin-tin spheres are expanded in spherical harmonics up to $l_{max}=10$, and the wave function in the interstitial region is expanded with plane waves up to $K_{max} = 7/R_{MT}$, where R_{MT} is the smallest muffin-tin sphere radius. R_{MT} 's were set as 2.00 (a.u.) for K and 1.23 (a.u.) for Oxygen, respectively. The charge density was expanded with plane waves up to $G_{max}=12$ (a.u.)⁻¹. We have used 200 k-points inside the first Brillouin zone. For [R1] and [R2] in Fig. 1, the O_2^- molecular bonds were assumed to be rotated uniformly by 30° from [T] structure around the [100] and [110] axis, respectively. The experimental lattice parameters $a=4.030\text{\AA}$ and $c=6.697\text{\AA}$ and the bond length $d_{oo}=1.306\text{\AA}$ were used.¹⁶ The spin direction was chosen to be perpendicular to the molecular axis following the experiment.⁵

Figure 2 provides the density of states (DOS) in the GGA band calculation for the FM phase of KO_2 with the high symmetry un-rotated structure [T]. Oxygen $2p$ partial DOS (PDOS) shows clear molecular level splittings among σ_g, π_u, π_g and σ_u in agreement with literature.² The finite DOS at the Fermi level E_F in the minority spin π_g states produces the half-metallic character for KO_2 ,

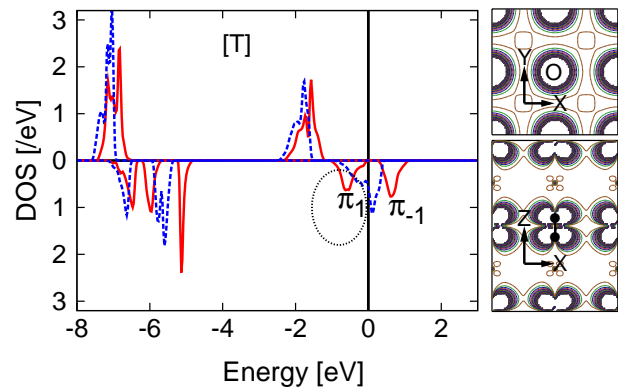


FIG. 3: (Color online) The PDOS of oxygen $2p$ states for the FM phase of KO_2 with [T] structure. The dotted (blue) and solid (red) lines represent the DOSs in the GGA+ U and the GGA+ U +SO, respectively ($U=6.53$ eV). The π_g states split into $\pi_{m=1}, \pi_{m=-1}$ in the GGA+ U +SO. Charge densities of $\pi_{m=1}$ states are plotted on the xy (001) (the upper panel) and on the xz (010) plane (the lower panel).

which reflects the failure of the GGA. The degenerate π_g states, which are composed of anti-bonding π_x and π_y states, should split for an insulating phase of KO_2 . To understand the splitting mechanism of the π_g states, we have considered the effects of the SO and the Coulomb correlation of O $2p$ electrons. The importance of the Coulomb correlation effect of O $2p$ electrons was examined recently in a similar $2p$ magnetic oxide Rb_4O_6 .^{17,18}

Figure 3 shows the DOS both in the GGA+ U and GGA+ U +SO for the FM phase of KO_2 with [T] structure. Note that the π_g states near E_F do not split in the GGA+ U with $U=6.53$ eV. They become split only when the SO is included in the GGA+ U : π_g split into $\pi_{m=1}$ and $\pi_{m=-1}$ which are mixed states of π_x and π_y . In the right of Fig. 3, the charge densities for the occupied $\pi_{m=1}$ states are plotted on the (001) and (010) planes. These charge densities manifest the azimuthally symmetric nature of $\pi_{m=1}$ states, which demonstrates that the splitting of π_g states originates from the SO effect. In fact, the large SO effect results from the Coulomb correlation, which localizes the $2p$ electrons to generate the substantial orbital magnetic moment in the π_g states. The magnitude of the orbital magnetic moment is as much as $0.570 \mu_B$ per O_2^- molecule, which is comparable to that of the spin magnetic moment of $1.0 \mu_B$. The direction of the orbital magnetic moment turns out to be almost parallel to the molecular axis, *i.e.*, perpendicular to that of the spin magnetic moment. We have checked that the electronic structure of AFM KO_2 with [T] structure is close to that of FM KO_2 , and so the band gap at E_F opens in the same way.

For KO_2 with [R1] and [R2] structures, the crystal field effect will be activated due to tilting of O_2^- molecular axes toward K^+ . Figure 4(a) shows the local PDOSs and the spin densities in the GGA+ U +SO for the AFM phase of KO_2 with [R1] structure. Notable feature in

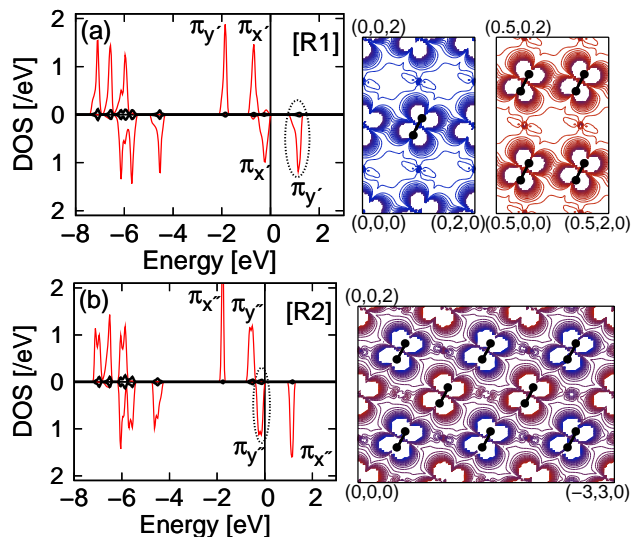


FIG. 4: (Color online) (a) The local PDOS of the O $2p$ states in the GGA+ U +SO ($U=6.53$ eV) for the AFM phase of KO_2 with [R1] structure. The spin densities of unoccupied $\pi_{y'}$ states are plotted on the (100) and (200) planes. Blue and red colors in the spin densities represent opposite spins. (b) The local PDOS of the O $2p$ states in the GGA+ U +SO ($U=6.53$ eV) for the AFM phase of KO_2 with [R2] structure. The spin density of occupied minority spin $\pi_{y''}$ states is plotted on the (110) plane. Black solid lines in the DOS plots represent the PDOS of K $4p$ states.

the DOS is the opening of band gap at E_F . The GGA band calculation does not produce the band gap, whereas both the GGA+ U and the GGA+ U +SO yield almost the same insulating band structure. This implies that, in producing the band gap, (i) the symmetry lowering just by tilting of molecular axes is not sufficient, (ii) the Coulomb correlation effect is essential, and (iii) the SO effect for [R1] is not as important as that for [T]. The orbital magnetic moment is almost quenched having only $0.002 \mu_B$ per O_2^- molecule. Therefore, it is the combined effect of the Coulomb U and the crystal field from K^+ cations that splits the degenerate π_g states into the directional orbitals, $\pi_{x'}$ and $\pi_{y'}$ states. Interestingly, due to the complex interplay of the Coulomb U and the crystal field effect in the molecular states, the splitting of π_g

TABLE I: Magnetic exchange constants [meV] between O_2^- molecules for direct and indirect (*via* K^+) hopping channels in the [R1] and [R2] structures of KO_2 . J_1 and J_2 are the in-plane exchange constants along the x and the y -direction, and J_3 is the inter-plane exchange constant. Positive J represents the AFM interaction.

	J_1	J_2	J_3
R1 (direct)	0.353	1.486	0.209
R1 (<i>via</i> K^+)	0.023	0.023	0.027
R2 (direct)	0.419	0.419	0.680
R2 (<i>via</i> K^+)	-0.215	-0.215	0.005

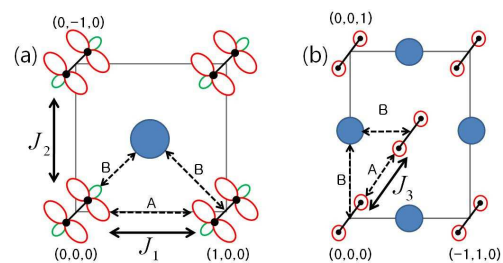


FIG. 5: (Color online) (a) The in-plane exchange constants, J_1 and J_2 , on the xy -plane for KO_2 with [R2], where the unoccupied $\pi_{x''}$ and occupied $\pi_{y''}$ states are represented by red and green, respectively. (b) The inter-plane exchange constant J_3 on the (110) plane. The paths A and B correspond to the direct and indirect (*via* K^+) hopping channels, respectively.

states occurs extraordinarily, *i.e.*, the $\pi_{y'}-\pi_{x'}$ order for the majority spin and the opposite $\pi_{x'}-\pi_{y'}$ order for the minority spin states. The half-filled molecular states $\pi_{y'}$ seem to be strongly affected by Coulomb U , while the fully occupied molecular states $\pi_{x'}$ seem to be weakly affected. The spin densities of unoccupied π_g states plotted on the (100) and (200) planes demonstrate that they really correspond to the $\pi_{y'}$ states. The $\pi_{y'}$ states in each plane exhibit the FM spin and ferro-orbital (FO) orderings, while they exhibit the inter-plane AFM spin ordering. Namely, the AFM and FO orderings take place concurrently.

Similarly, Fig. 4(b) shows the local PDOSs and the spin densities in the GGA+ U +SO for AFM KO_2 with [R2] structure. For [R2] too, the GGA does not produce the band gap, whereas both the GGA+ U and the GGA+ U +SO produce it. The SO effect is again negligible so that the orbital magnetic moment is quenched having only $0.008 \mu_B$ per O_2^- molecule. Degenerate π_g states are split into $\pi_{x''}$ and $\pi_{y''}$ due to the combined effect of the Coulomb U and the crystal field from K^+ . The spin density of occupied minority spin π_g states plotted on the (110) plane demonstrates that they really correspond to the $\pi_{y''}$ states.

Now let us examine the magnetic interaction in KO_2 based on the above electronic structures. The implication of Fig. 4 is that, with the tilting of O_2^- molecular axes in the AFM [R1] and [R2] structures, the band gap opening and the FO ordering in π_g states occur simultaneously. According to the spin-orbital model for $3d$ transition-metal (TM) oxides,¹⁹ the FO ordering of TM $3d$ states would induce the AFM superexchange interaction between two TM spins, and vice versa. In this respect, the results in Fig. 4 look reasonable. The superexchange, more generally, the kinetic exchange in KO_2 will take place through two channels: the direct hopping between two O_2^- molecules and the indirect hopping *via* K^+ (see Fig. 5). The unoccupied K $4p$ states are located 4–6 eV above E_F (see Fig. 2), and so there is a possibility of hopping mechanism through $\text{O}_2^--\text{K}^+-\text{O}_2^-$. Indeed,

as revealed in Fig. 4, there exists the nonnegligible hybridization between the O $2p$ and K $4p$ states.

Table I presents the estimated exchange constants based on the microscopic calculation of the kinetic exchange interaction for KO_2 with the [R1] and [R2] structures.²⁰ The $2p$ electrons in each O_2^- are assumed to have the atomic orbital states as in our band results for [R1] and [R2]. The kinetic exchange interactions both from the direct and indirect hoppings were considered independently to calculate the exchange constant for each channel. For [R1], the exchange constants are obtained to be all AFM, and the dominant channel is the direct hopping between O_2^- anions along the y -direction, which is AFM ($J_2=1.486$ meV). The large J_2 results from the tilting of O_2^- molecular axis along the [010]. The inter-plane interactions from both direct and indirect channels yield smaller exchange constants ($J_3=0.209$ and 0.027 meV). Then the resulting magnetic structure for [R1] will not be consistent with the experimental AFM structure which has alternating AFM spins along [001].

On the other hand, the kinetic exchange interactions for [R2] turn out to be consistent with the experimental AFM structure. The dominant one is the inter-plane AFM interaction coming from the direct hopping ($J_3=0.680$ meV). The in-plane exchange constants are 0.419 and -0.215 meV for direct and indirect channels, respectively. Hence the total exchange constants between two nearest neighbor (NN) O_2^- along x and y -directions are 0.204 meV. For each O_2^- in [R2], there are eight inter-plane NN O_2^- and four in-plane NN O_2^- . As a consequence, much larger J_3 than J_1 and J_2 will generate the interlayer AFM ordering along [001], as is consistent with the experimental AFM structure.

The in-plane FM interactions (-0.215 meV) coming from the indirect hopping *via* K^+ play an important role in stabilizing the in-plane FM ordering. As shown in

Fig. 5(a), out of two neighboring O_2^- molecules on the xy plane in [R2], the lobes of $\pi_{x''}$ orbital of one molecule are toward the intermediate K^+ , while those of the other molecule are away from K^+ and thereby the lobes of $\pi_{y''}$ orbital are toward the intermediate K^+ . This arrangement of the orbitals suggests that the hopping takes place between the occupied $\pi_{y''}$ and unoccupied $\pi_{x''}$ orbitals of two neighboring O_2^- molecules. This is reminiscent of the resulting FM superexchange interaction between the fully-occupied and half-filled orbitals in TM oxides in the framework of the Goodenough-Kanamori-Anderson (GKA) rule.²¹ In contrast, for the inter-plane kinetic exchange in Fig. 5(b), the lobes of $\pi_{x''}$ orbitals of both O_2^- molecules are away from K^+ , and so the indirect kinetic exchange results in the weak AFM interaction ($J_3=0.005$ meV).

In conclusion, we have investigated electronic and magnetic structures of KO_2 superoxide, the strongly correlated $2p$ electron system. We have found that, for the correct description of the insulating electronic structure of KO_2 , the SO coupling as well as the large Coulomb correlation is important for the high symmetry phase, while, for the low symmetry phase, the crystal field from K^+ , as well as the large Coulomb correlation, is important. The concurrent AFM spin and FO orderings with the band-gap opening clearly demonstrate the strong coupling among the spin-orbital-lattice degrees of freedom in KO_2 . In the low symmetry phase of KO_2 with [R2] structure, the emergent FO ordering yields the kinetic exchange interactions that are consistent with the experimental AFM structure.

This work was supported by the NRF (No.2009-0079947), and by the POSTECH Research Fund. Helpful discussions with Y. H. Jeong and J.-S. Kang are greatly appreciated.

-
- ¹ J. J. Attema, G. A. de Wijs, and R. A. de Groot, *J. Phys.: Condens. Matter*, **19**, 165203 (2007).
² I. V. Solovyev, *New J. Phys.* **10**, 013035 (2008).
³ R. J. Meier and R. B. Helmholdt, *Phys. Rev. B* **29**, 1387 (1984).
⁴ W. Känzig and M. Labhart, *J. Phys. (paris)* **37**, C7-39 (1976).
⁵ M. Labhart, D. Raoux, W. Känzig, and M. A. Bösch, *Phys. Rev. B* **20**, 53 (1979).
⁶ W. Hesse, M. Jansen, and W. Schnick, *Prog. Solid State Chem.* **19**, 47 (1989).
⁷ J. J. Attema, G. A. de Wijs, G. R. Blake, and R. A. de Groot, *J. Am. Chem. Soc.* **127**, 16325 (2005).
⁸ M. A. Bösch, M. E. Lines, and M. Labhart, *Phys. Rev. Lett.* **45**, 140 (1980).
⁹ M. E. Lines and M. A. Bösch, *Phys. Rev. B* **23**, 263 (1981).
¹⁰ H. G. Smith, R. M. Nicklow, L. J. Raubenheimer, and M. K. Wilkinson, *J. Appl. Phys.* **37** 1047 (1966)
¹¹ G. Kemeny, T. A. Kaplan, S. D. Mahanti, and D. Sahu, *Phys. Rev. B* **24**, 5222 (1981).
¹² M. E. Lines, *Phys. Rev. B* **24**, 5248 (1981).
¹³ M. Weinert, E. Wimmer, and A. J. Freeman, *Phys. Rev. B* **26**, 4571(1982).
¹⁴ P. Blaha, K. Schwarz, G.K.H. Madsen, D. Kvasnicka, J. Luitz, WIEN2k (Karlheinz Schwarz, Technische Universität Wien, Austria, 2001).
¹⁵ J. P. Perdew, K. Burke and M. Ernzerhof, *Phys. Rev. Lett.* **77**, 3865 (1996).
¹⁶ Since the triclinic deformation is very small for [R1] and [R2], we assumed the tetragonal structure in the band calculations. See Ref.⁴.
¹⁷ J. Winterlik, G. H. Fecher, and C. Felser, *J. Am. Chem. Soc.*, **129**, 6990 (2007).
¹⁸ J. Winterlik, G. H. Fecher, C. A. Jenkins, C. Felser, C. Mühle, K. Doll, M. Jansen, L. M. Sandratskii, and J. Kübler, *Phys. Rev. Lett.* **102**, 016401 (2009).
¹⁹ K. I. Kugel and D. I. Khomskii, *Sov. Phys. Usp.* **25**, 231 (1982).
²⁰ B. H. Kim, Ph.D. Thesis, (POSTECH 2009).
²¹ J. B. Goodenough, *Magnetism and the Chemical Bond*,

Interscience Publ., N.Y.-Lnd., (1976)